Ultra-high-speed optical serial-to-parallel data conversion by time-domain optical Fourier transformation in a silicon nanowire

Mulvad, Hans Christian Hansen; Palushani, Evarist; Hu, Hao; Ji, Hua; Lillieholm, Mads; Galili, Michael; Clausen, Anders; Pu, Minhao; Yvind, Kresten; Hvam, Jørn Märcher

Published in:
Optics Express

Link to article, DOI:
10.1364/OE.19.00B825

Publication date:
2011

Document Version
Publisher's PDF, also known as Version of record

Ultra-high-speed optical serial-to-parallel data conversion by time-domain optical Fourier transformation in a silicon nanowire

Hans Christian, Hansen Mulvad,* Evarist Palushani, Hao Hu, Hua Ji, Mads Lillieholm, Michael Galili, Anders T. Clausen, Minhao Pu, Kresten Yvind, Jørn M. Hvam, Palle Jeppesen, and Leif K. Oxenløwe

DTU Fotonik, Department of Photonics Engineering, Technical University of Denmark, Building 343, DK-2800 Kgs. Lyngby, Denmark
hchm@fotonik.dtu.dk

Abstract: We demonstrate conversion from 64 × 10 Gbit/s optical time-division multiplexed (OTDM) data to dense wavelength division multiplexed (DWDM) data with 25 GHz spacing. The conversion is achieved by time-domain optical Fourier transformation (OFT) based on four-wave mixing (FWM) in a 3.6 mm long silicon nanowire. A total of 40 out of 64 tributaries of a 64 × 10 Gbit/s OTDM-DPSK data signal are simultaneously converted with a bit-error rate (BER) performance below the 2×10^{-3} FEC limit. Using a 50 m long highly nonlinear fiber (HNLF) for higher FWM conversion efficiency, 43 tributaries of a 64 × 10 Gbit/s OTDM-OOK data signal are converted with error-free performance ($BER<10^{-9}$).

OCIS codes: (060.4510) Optical communications; (190.4380) Nonlinear optics, four-wave mixing.

References and links

1. P. J. Winzer, G. Raybon, C. R. Doerr, M. Duelk, and C. Dorrer, "107 Gb/s optical signal generation using electronic time-division multiplexing," J. Lightwave Technol. **24**(8), 3107–3113 (2006).
2. C. Schubert, R. H. Derksen, M. Möller, R. Ludwig, C.-J. Weiske, J. Lutz, S. Ferber, and C. Schmidt-Langhorst, "107 Gbit/s transmission using an integrated ETDM receiver," *European Conference on Optical Communication, ECOC 2006*, Cannes, France, September 2006, paper Tu1.5.5 (2006).
3. H. C. Hansen Mulvad, L. K. Oxenløwe, M. Galili, A. T. Clausen, L. Grüner-Nielsen, and P. Jeppesen, "1.28 Tbit/s single-polarisation serial OOK optical data generation and demultiplexing," Electron. Lett. **45**(5), 280–281 (2009).
4. T. Richter, E. Palushani, C. Schmidt-Langhorst, M. Nölle, R. Ludwig, and C. Schubert, "Single wavelength channel 10.2 Tb/s TDM-data capacity using 16-QAM and coherent detection," in *Optical Fiber Communication Conference*, OSA Technical Digest (CD) (Optical Society of America, 2011), paper PDPA9.
5. A. E. Willner, O. F. Yilmaz, J. Wang, X. Wu, A. Bogoni, L. Zhang, and S. R. Nuccio, "Optically efficient nonlinear signal processing," IEEE J. Sel. Top. Quantum Electron. **17**(2), 320–332 (2011).
6. R. S. Tucker and K. Hinton, "Energy consumption and energy density in optical and electronic signal processing," IEEE Photon. J. **3**(5), 821–833 (2011).
7. H. Hu, H. Ji, M. Galili, M. Pu, C. Peucheret, H. Christian H Mulvad, K. Yvind, J. M. Hvam, P. Jeppesen, and L. K. Oxenløwe, "Ultra-high-speed wavelength conversion in a silicon photonic chip," Opt. Express **19**(21), 19886–19894 (2011).
8. S. Watanabe, F. Futami, R. Okabe, Y. Takita, S. Ferber, R. Ludwig, C. Schubert, C. Schmidt, and H. G. Weber, "160 Gbit/s optical 3R-regenerator in a fiber transmission experiment," in *Optical Fiber Communication Conference*, Technical Digest (Optical Society of America, 2003), paper PD16.
9. K. Uchiyama, H. Takara, K. Mori, and T. Morioka, "160 Gbit/s all-optical time-division demultiplexing utilising modified multiple-output OTDM demultiplexer (MOXIC)," Electron. Lett. **38**(20), 1190–1191 (2002).
10. C.-S. Brès, A. O. J. Wiberg, B. P.-P. Kuo, J. M. Chavez-Boggio, C. F. Marki, N. Alic, and S. Radic, "Optical demultiplexing of 320 Gb/s to 8×40 Gb/s in single parametric gate," J. Lightwave Technol. **28**(4), 434–442 (2010).
11. K. J. Lee, S. Liu, F. Parmigiani, M. Ibsen, P. Petropoulos, K. Gallo, and D. J. Richardson, "OTDM to WDM format conversion based on quadratic cascading in a periodically poled lithium niobate waveguide," Opt. Express **18**(10), 10282–10288 (2010).

#157928 - $15.00 USD Received 9 Nov 2011; revised 30 Nov 2011; accepted 1 Dec 2011; published 6 Dec 2011

12. H. N. Tan, Q. Nguyen-The, M. Matsuura, and N. Kishi, "Wavelength- and time-selective OTDM-to-WDM conversion with variable channel spacing in WDM grid using a reconfigurable multiwavelength pulse compressor," *European Conference on Optical Communication, ECOC 2011*, Geneva, Switzerland, September 18–22, 2011, paper Tu.5.LeCervin.2 (2011).
13. H. C. Hansen Mulvad, E. Palushani, M. Galili, J. Xu, H. Hu, A. Clausen, L. Oxenløwe, and P. Jeppesen, "OTDM-WDM conversion based on time-domain optical Fourier transformation with spectral compression," in *Optical Fiber Communication Conference*, OSA Technical Digest (CD) (Optical Society of America, 2011), paper OThN2.
14. E. Palushani, H.C.H. Mulvad, M. Galili, H. Hu, L.K. Oxenløwe, A. Clausen, and P. Jeppesen, "OTDM-to-WDM conversion based on time-to-frequency mapping by time-domain optical Fourier transformation," IEEE J. Sel. Top Quantum Electron. **PP**(99), 1–8, DOI: 10.1109/JSTQE.2011.2131121 (2011).
15. H. C. Hansen Mulvad, P. Guan, K. Kasai, T. Hirooka, and M. Nakazawa, "High-resolution 640 Gbit/s clock recovery using time-domain optical Fourier transformation and narrowband optical filter," *European Conference on Optical Communication, ECOC 2010*, Turin, Italy, September 2010, paper Mo.1.A.6 (2010).
16. P. Guan, H. C. Hansen Mulvad, K. Kasai, T. Hirooka, and M. Nakazawa, "High time-resolution 640-Gb/s clock recovery using time-domain optical Fourier transformation and narrowband optical filter," IEEE Photon. Technol. Lett. **22**(23), 1735–1737 (2010).
17. H. C. Hansen Mulvad, E. Palushani, H. Hu, H. Ji, M. Galili, A. T. Clausen, M. Pu, K. Yvind, J. M. Hvam, P. Jeppesen, and L. K. Oxenløwe, "Ultra-high-speed optical serial-to-parallel data conversion in a silicon nanowire," *European Conference on Optical Communication, ECOC 2011*, Geneva, Switzerland, September 18–22, 2011, postdeadline paper Th.13.A.2 (2011).
18. M. A. Foster, A. C. Turner, R. Salem, M. Lipson, and A. L. Gaeta, "Broad-band continuous-wave parametric wavelength conversion in silicon nanowaveguides," Opt. Express **15**(20), 12949–12958 (2007).
19. M. A. Foster, R. Salem, D. F. Geraghty, A. C. Turner-Foster, M. Lipson, and A. L. Gaeta, "Silicon-chip-based ultrafast optical oscilloscope," Nature **456**(7218), 81–84 (2008).
20. H. Ji, M. Pu, H. Hu, M. Galili, L. K. Oxenløwe, K. Yvind, J. M. Hvam, and P. Jeppesen, "Optical waveform sampling and error-free demultiplexing of 1.28 Tb/s serial data in a nanoengineered silicon waveguide," J. Lightwave Technol. **29**(4), 426–431 (2011).
21. B. H. Kolner and M. Nazarathy, "Temporal imaging with a time lens," Opt. Lett. **14**(12), 630–632 (1989).
22. M. Nakazawa, T. Hirooka, F. Futami, and S. Watanabe, "Ideal distortion-free transmission using optical Fourier transformation and Fourier transform-limited optical pulses," IEEE Photon. Technol. Lett. **16**(4), 1059–1061 (2004).
23. C. V. Bennett and B. H. Kolner, "Principles of parametric temporal imaging—part I: system configurations," IEEE J. Quantum Electron. **36**(4), 430–437 (2000).
24. K. G. Petrillo and M. A. Foster, "Scalable ultrahigh-speed optical transmultiplexer using a time lens," Opt. Express **19**(15), 14051–14059 (2011).
25. M. Pu, L. Liu, H. Ou, K. Yvind, and J. M. Hvam, "Ultra-low-loss inverted taper coupler for silicon-on-insulator ridge waveguide," Opt. Commun. **283**(19), 3678–3682 (2010).
26. M. Pu, H. Hu, M. Galili, H. Ji, C. Peucheret, L. Oxenløwe, K. Yvind, P. Jeppesen, and J. Hvam, "15-THz tunable wavelength conversion of picosecond pulses in a silicon waveguide," IEEE Photon. Technol. Lett. **23**(19), 1409–1411 (2011).
27. M. Jinno, "Effects of crosstalk and timing jitter on all-optical time-division demultiplexing using a nonlinear fiber Sagnac interferometer switch," IEEE J. Quantum Electron. **30**(12), 2842–2853 (1994).
28. F. Futami, Y. Takushima, and K. Kikuchi, "Generation of 10 GHz, 200 fs Fourier-transform-limited optical pulse train from modelocked semiconductor laser at 1.55 μm by pulse compression using dispersion-flattened fibre with normal group-velocity dispersion," Electron. Lett. **34**(22), 2129–2130 (1998).
29. C. G. Joergensen, T. Veng, L. Grüner-Nielsen, and M. Yan, "Dispersion flattened highly non-linear fiber," *29th European Conference on Optical Communication, ECOC 2003*, September 21–23, Rimini, Italy, paper We3.7.6 (2003).
30. E. Palushani, L. K. Oxenløwe, M. Galili, H. C. Hansen Mulvad, A. T. Clausen, and P. Jeppesen, "Flat-top pulse generation by the optical Fourier transform technique for ultrahigh speed signal processing," IEEE J. Quantum Electron. **45**(11), 1317–1324 (2009).

1. Introduction

The rapid growth in Internet traffic is approaching the capacity limits of modern communication networks while also being accompanied by increasing energy consumption. Hence, there is an extensive ongoing research effort into developing communication systems with both higher capacity and a more energy-efficient operation. A possible approach is to increase the single-channel bit rates in order to realize simpler systems by way of fewer wavelength channels. Presently, single channels are created by electrical time-division multiplexing (ETDM) followed by electro-optic encoding onto an optical channel. The speed of ETDM has been pushed to ~100 Gbit/s for signal generation and detection, as demonstrated in research laboratories [1, 2]. On the other hand, optical time-division multiplexing (OTDM) allows for the generation of single-channel bit rates beyond 1 Tbit/s [3,

#157928 - $15.00 USD Received 9 Nov 2011; revised 30 Nov 2011; accepted 1 Dec 2011; published 6 Dec 2011

4], which is far above the limits for electrical detection and processing. Such high data rates rely on optical signal processing (OSP), which is based on nonlinear optical effects with intrinsic response times down to a few femtoseconds allowing for operation speeds of several Tbit/s. Compared to electrical signal processing (ESP), OSP has the capability to transparently process data regardless of the bit rate, thus enabling a scaling of the operation speed without an associated increase in energy consumption [5]. Hence, OSP is being actively pursued as a possible technology in future communication systems, but the exact role remains to be determined. At low data rates, electrical solutions still remain superior to optical alternatives both in terms of versatility, performance and cost. Instead, OSP appears better suited for much higher data rates where it can allow for large amounts of data to be processed simultaneously in a single device with an associated low switching energy per bit [6]. Examples of this type of OSP are wavelength conversion [7] or regeneration [8]. For such OSP functionalities, the potentially lowest energy per bit could be obtained for the ultra-high-speed serial rates that can be generated by OTDM. A high-speed OTDM signal is simply formed by time-interleaving a large number of data tributaries at a low rate of e.g. 10 Gbit/s, each based on low duty-cycle optical pulses at the same wavelength [3]. On the other hand, receiving an OTDM signal is a challenging task. Here, the femtosecond response time of OSP is essential for time-demultiplexing the data tributaries in order to enable their electrical detection. However, typical OTDM demultiplexers extract only a single tributary [3, 4], implying a highly complex and therefore energy-consuming receiver structure in order to detect the full data content. To overcome this challenge, many schemes have been proposed for demultiplexing all or several tributaries in a single optical device by serial-to-parallel conversion of the OTDM tributaries to wavelength division multiplexed (WDM) channels [9–12]. Similarly to OTDM wavelength conversion, serial-to-parallel conversion processes large number of data in a single device which should bring down the required energy per bit. Indeed, a simple and bit-rate scalable OTDM-WDM converter could be an enabling technique for ultra-high speed serial data communication systems with potentially moderate energy requirements. To our knowledge, earlier OTDM-WDM conversion techniques preserve the spectral width of the converted tributaries, and are therefore hardly bit-rate scalable since a huge bandwidth would be required for ultra-high speed OTDM data with high multiplicity. Previously, we have proposed time-domain Optical Fourier transformation (OFT) for a spectrally efficient and thus scalable OTDM-WDM conversion, since it allows a simultaneous spectral compression of the tributaries with direct mapping onto a dense WDM grid (DWDM) [13]. In principle, more than half of all OTDM tributaries can be converted in a single OFT device, meaning that all tributaries may be simultaneously demultiplexed by conversion to DWDM with only two parallel OFT devices [14]. The technique was first employed in an OTDM clock recovery demonstration, where 640 Gbit/s time-resolution was achieved by electro-optic phase-modulation with only 40 GHz bandwidth [15, 16]. Later, OTDM-DWDM conversion of 32 × 10 Gbit/s and 64 × 10 Gbit/s OTDM data was demonstrated using four-wave mixing (FWM) based phase-modulation in highly nonlinear fiber (HNLF), but with less than 10 converted tributaries at a relatively large (≥100 GHz) DWDM spacing [13, 14].

In this paper, we demonstrate the first optical serial-to-parallel conversion in a silicon nanowire using FWM-based time-domain OFT [17]. Additionally, the full potential of the technique is demonstrated by converting more than half of 64 × 10 Gbit/s OTDM data tributaries to a dense 25 GHz DWDM spacing. As a platform for OSP, nonlinear silicon photonics is attracting considerable interest due to its complementary metal–oxide–semiconductor (CMOS) compatibility, integration potential with electronics, low cost and broad operation bandwidth [7, 18–20]. In the present demonstration, 40 out of 64 consecutive 10 Gbit/s tributaries in a 640 Gbit/s OTDM-DPSK data signal are converted onto a 25 GHz DWDM grid. The BER performance is within the standard FEC limit of 2×10^{-3}, being limited by the FWM conversion efficiency of our silicon sample. We also perform a demonstration on 640 Gbit/s OTDM-OOK data in a 50 m HNLF, where the higher FWM conversion efficiency enables error-free performance (BER<10^{-9}) for 43 out of 64 tributaries converted to 25 GHz DWDM.

#157928 - $15.00 USD Received 9 Nov 2011; revised 30 Nov 2011; accepted 1 Dec 2011; published 6 Dec 2011

2. Principle of operation

Time-domain OFT is equivalent to the so-called time-lens technique which originates in the space-time duality between diffractive propagation of spatial beams of light and dispersive propagation of temporal pulses of light [21]. In the spatial system, a lens can be employed to achieve a spatial Fourier transformation of an object placed at the front focal plane. The temporal equivalent of a spatial lens is a quadratic phase-modulation as a function of time, denoted a "time-lens". When combined with dispersive propagation, a time-lens allows a Fourier transformation that can transfer the spectral profile of a pulsed waveform into the time-domain and vice-versa [22]. The time-domain OFT setup for a time-to-frequency transformation is shown in Fig. 1(a), where it converts time-interleaved OTDM tributaries into frequency-interleaved DWDM channels.

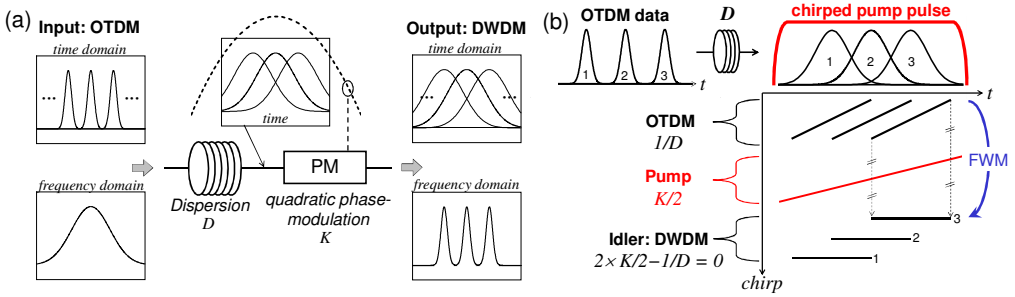

Fig. 1. (a) Principle of time-domain OFT for OTDM-DWDM conversion under the condition $D = 1/K$, (b) chirp vs time diagram of the FWM-based quadratic phase-modulation for the OFT: after dispersion (D), the OTDM pulses are combined with the linearly chirped pump pulse to generate the idler DWDM signal by FWM (chirp rates are denoted below the 3 signals).

Firstly, the OTDM pulses are propagated through a medium with accumulated second order chromatic dispersion D, given by $D = \beta_2 L$ for a medium of length L and second order dispersion parameter β_2. By propagating through the dispersive medium, the pulses broaden and acquire a linear chirp. The acquired chirp rate can be approximated by $1/D$ when the pulses are propagated well beyond their dispersion length. Subsequently, the broadened pulses receive a quadratic phase-modulation at a rate K so as to cancel the dispersive chirp, resulting in a spectral compression. The dispersion and chirp must be balanced according to the condition $D = 1/K$ in order to achieve a successful time-to-frequency mapping. Under such conditions, OTDM tributaries interleaved by a temporal spacing $\Delta\tau$ are transformed to DWDM channels with frequency spacing Δf according to the equation $2\pi \times \Delta f = K \times \Delta\tau$. A more detailed analysis can be found in [14, 16].

The phase-modulation must operate at the base rate of the tributaries, in order to map each pulse of a tributary to the same specific DWDM wavelength. In this paper, the base rate is 10 GHz and the target is to map a 640 Gbit/s tributary spacing of $\Delta\tau$ = 1.56 ps to a DWDM spacing Δf = 25 GHz, which requires K = 0.1 ps^{-2} and D = 10 ps^2. A Gaussian pulse with full-width at half maximum width (FWHM) of 615 fs is employed for the 640 Gbit/s data. Such a pulse is broadened to a FWHM of ~45 ps after the dispersive medium. Generating the required linear chirp over such a relatively large time span requires phase-modulation by a parametric process such as FWM [19, 23]. Indeed, the typically used electro-optical sinusoidal phase-modulation [16, 22] is approximately quadratic only for about 15-20% of the period, corresponding to 15-20 ps for a 10 GHz sine. The FWM-based phase modulation process is shown in Fig. 1(b), in terms of a schematic chirp vs. time diagram. Linearly chirped pulses of chirp rate $K/2$ serve as pump signal (field $E_p(t)$), and the dispersed OTDM pulses with chirp rate $1/D$ act as probe signal (field $E_s(t)$). The FWM process will generate an idler field $E_i(t) \propto E_p^2(t)\, E_s^*(t)$ where the pump and OTDM phases are combined. The idler chirp rate is thus given by $2 \times K/2 - 1/D$, which is zero since the condition $D = 1/K$ is fulfilled. In this way, the DWDM tributaries are obtained in the idler signal after the conversion process.

#157928 - $15.00 USD Received 9 Nov 2011; revised 30 Nov 2011; accepted 1 Dec 2011; published 6 Dec 2011

With the FWM method, quadratic phase-modulation is obtained over the temporal extent of the pump pulse, which also determines the number of convertible OTDM tributaries. The dispersed tributaries that are not fully overlapped by the pump pulse will be distorted in the conversion process. The tributaries crossing the tails of the pump pulse will suffer from lower conversion efficiency as well as a broadening of the DWDM channel spectrum, leading to reduced optical signal to noise ratio (OSNR) and DWDM inter-channel cross-talk, respectively. By employing a flat-top pump pulse extending to nearly the entire base rate bit slot, the number of successfully converted tributaries is maximised and can exceed 50% in this case [14]. An independent numerical study of the same technique by Petrillo and Foster indicates that all tributaries can be converted without cross-talk when using OTDM pulses with sufficiently low duty cycle and a higher target DWDM spacing of 100 GHz [24]. In their work, the larger temporal gap between neighbouring tributary pulses is OFT-converted to a guard band between DWDM channels that should accommodate for the above-mentioned spectral broadening (our interpretation).

3. Experimental setup

Two separate experimental demonstrations are carried out: 1) conversion of 640 Gbit/s OTDM encoded with differential phase-shift keying (DPSK) to 25 GHz DWDM using a silicon nanowire, and 2) conversion of 640 Gbit/s OTDM encoded with on-off keying (OOK) to 25 GHz DWDM using a standard HNLF. The experimental setup is shown in Fig. 2(a) and (b). Only the data format, the 10 Gbit/s receiver, and the FWM medium (silicon nanowire or HNLF) differ between the two cases. All other parameters are kept the same.

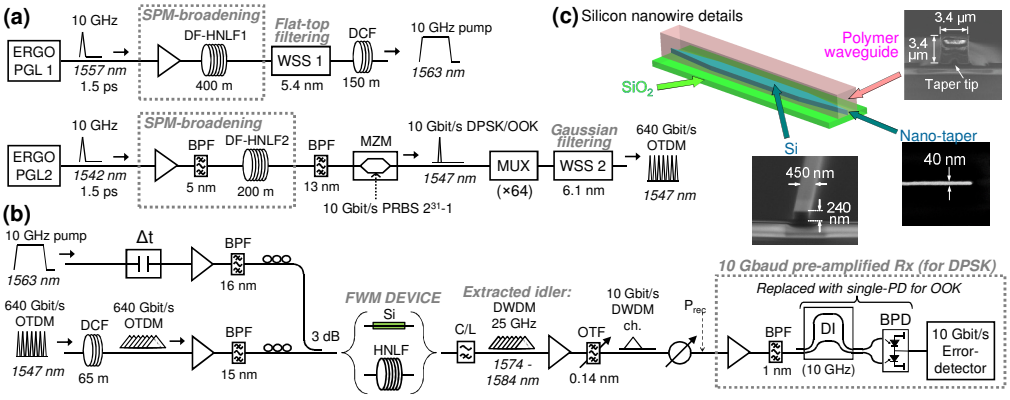

Fig. 2. (a), (b) Experimental setup. (c) Schematic drawing of the nano-engineered silicon nanowire and scanning electron micrograph pictures of the sample.

3.1 Details of the silicon nanowire and the HNLF

The silicon nanowire is depicted in Fig. 2(c) together with scanning electron micrograph pictures of various details. The device is a dispersion engineered straight 3.6-mm long silicon waveguide, which includes tapering sections for low-loss interfacing with optical fiber. The main waveguide section is ~3 mm long and has a cross section of 450 nm × 240 nm while the tapering sections are each ~0.3 mm long and their width is inversely tapered from 450 nm to 40 nm. This tapering enables coupling between the silicon waveguide and the larger polymer waveguide (SU8-2005) into which the whole silicon structure is embedded [25]. The cross section (3.4 × 3.4 μm^2) of the polymer waveguide matches the tapered access fibers, reducing the fiber coupling loss to 1.5 dB per facet. The device has a silicon-on-insulator (SOI) structure, with the silicon waveguide placed on a SiO_2/Si substrate. The measured propagation loss is 4.3 dB/cm and the fiber-to-fiber loss of the device is 4.5 dB. A FWM conversion bandwidth of more than 12 THz has been measured for this nanowire when using a CW pump in the C-band [7, 26]. The nonlinear loss is small (< 1 dB) when the coupled peak power is

#157928 - $15.00 USD Received 9 Nov 2011; revised 30 Nov 2011; accepted 1 Dec 2011; published 6 Dec 2011

relatively low, but increases dramatically when the coupled peak power exceeds a two-photon absorption (TPA) threshold around ~39 dBm, which is explained and characterized in [7]. Below this power level, the ultra-fast Kerr effect dominates and the silicon nanowire can be employed for FWM-based signal processing without significant TPA and free carrier absorption (FCA) induced patterning effects.

The details of the standard HNLF are as follows: length 50 m, nonlinear coefficient γ~10 $W^{-1}km^{-1}$, zero-dispersion wavelength ~1565 nm and dispersion slope 0.02 ps/(nm^2·km).

3.2 Generation of pump pulses and OTDM data

Figure 2(a) shows the setups for generating the pump pulses for the FWM process and the OTDM data signal. The pump and OTDM signal are obtained from 10 GHz erbium glass oscillating pulse-generating lasers at 1557 nm (ERGO-PGL1) and 1542 nm (ERGO-PGL2), respectively, both emitting ~1.5 ps FWHM pulses. The ERGO-PGLs, the PRBS pattern generator, and the 10 Gbit/s receiver are synchronized by a 10 GHz synthesizer with low phase-noise (Anritsu MG3691B), not shown in Fig. 2. The root mean square (RMS) timing jitter of the ERGO-PGL output pulses is ~50 fs, measured using an optical sampling oscilloscope (OSO). In general, a low pulse jitter is required in high-speed OTDM systems [27]. The low jitter level in our system would allow for an OTDM bit rate up to 1.28 Tbit/s [3]. It should be also noted that a practical system would require a clock recovery scheme to extract the 10 GHz base rate clock from an incoming transmitted OTDM signal, in order to synchronise the pump pulse source and the receiver, see e.g [15, 16].

The output pulses of both ERGO-PGLs undergo self-phase modulation (SPM) in dispersion-flattened highly nonlinear fibers (DF-HNLF) with normal dispersion, in order to generate broadened spectra with a flat-top envelope [28, 29]. To obtain the pump pulses, the output spectrum of DF-HNLF1 is filtered using a wavelength selective switch WSS1 (Finisar Waveshaper 4000S). The WSS is based on a programmable liquid crystal on silicon array that can control both the amplitude and phase of an input waveform as a function of frequency. The WSS1 is programmed with a 5th order super-Gaussian of 5.3 nm 3-dB bandwidth, centred at 1563 nm. The resulting flat-top output spectrum of WSS1 is shown in Fig. 3(a).

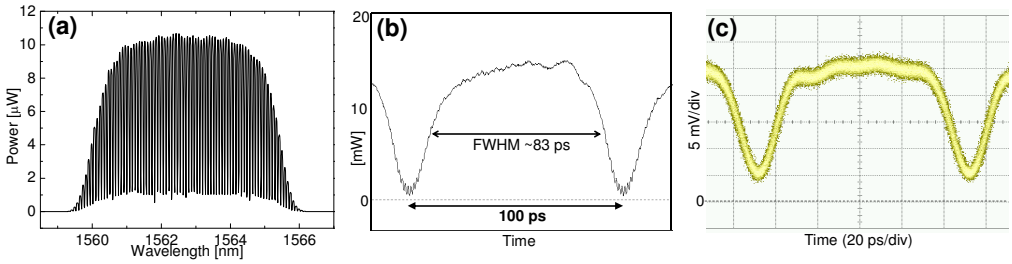

Fig. 3. Characterization of the 10 GHz pump pulse. (a) Optical spectrum, res. 0.01 nm. (b,c) Temporal shape at input to FWM medium measured using (b) OSO and (c) OSC.

The flat-top spectral shape can be transformed into the temporal domain by propagating the pulses through a sufficiently long dispersive medium, whereby a linear chirp is also acquired [30]. In this case, the WSS1 output pulses are propagated through a 150 m dispersion-compensating fiber (DCF), resulting in a linearly chirped waveform with a ~83 ps FWHM flat-top shape. An OSO trace of the pump pulse is shown in Fig. 3(b). Figure 3(c) shows the pulse on an electrical sampling oscilloscope (OSC) after photo-detection (~30 GHz bandwidth). The chirp rate as determined from the ratio between the spectral 3-dB width and the temporal FWHM is 0.05 ps^{-2}, which is the required pump chirp rate *K/2* for a FWM-based OFT conversion from 640 Gbit/s OTDM to 25 GHz DWDM.

To obtain the data signal, the output spectrum of DF-HNLF2 is filtered at ~1547 nm with a 13 nm optical band-pass filter (BPF). The resulting pulses are data-modulated with a 10 Gbit/s 2^{31}-1 PRBS pattern in a push-pull Mach-Zehnder modulator (MZM) to obtain either differential phase-shift keying (DPSK) or on-off keying (OOK) format. The data-modulated

#157928 - $15.00 USD Received 9 Nov 2011; revised 30 Nov 2011; accepted 1 Dec 2011; published 6 Dec 2011

pulses are subsequently multiplexed from 10 Gbit/s to 640 Gbit/s single-polarisation OTDM using passive fiber-based delay-line multiplexer stages (MUX). Finally, a second wavelength selective switch (WSS 2) is employed to shape the data spectrum into a Gaussian with ~6.1 nm 3-dB bandwidth at 1547 nm. A pulse autocorrelation of the resulting 640 Gbit/s OTDM signal (in the case of DPSK) is shown in Fig. 4(a). The autocorrelation of a single pulse can be fitted by an 870 fs FWHM Gaussian, corresponding to a nearly transform-limited Gaussian pulse with a FWHM of 615 fs. Figures 4(b) and (c) show OSO traces of the 640 Gbit/s OTDM-DPSK and 640 Gbit/s OTDM-OOK signals, respectively, where all the 64 constituent tributaries can be observed. Note that the time-resolution of the OSO is ~1 ps.

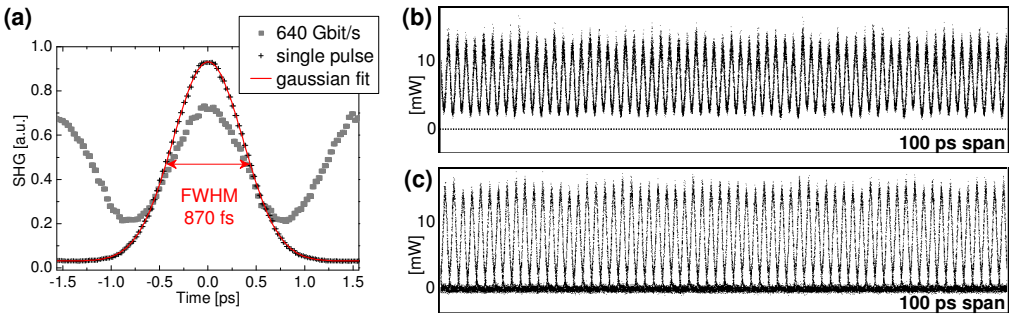

Fig. 4. Characterization of the OTDM signal (before OFT). (a) Pulse autocorrelations, (b) OSO trace of 640 Gbit/s OTDM-DPSK data, (c) OSO trace of 640 Gbit/s OTDM-OOK data.

3.3 OTDM-DWDM converter and 10 Gbit/s receiver

The generated pump and OTDM signals from Fig. 2(a) enter the setup for OTDM-DWDM conversion shown in Fig. 2(b). As the first step in the OFT process, the OTDM pulses are dispersed in a 65 m DCF (*D*). The OTDM and pump signals are then amplified, filtered, and combined using a 3 dB coupler before undergoing FWM in either the silicon nanowire or the HNLF. The average input power to the tapered fiber before the silicon nanowire is 22.0 dBm for the pump and 12.6 dBm for the OTDM signal. The same power levels are used as input to the HNLF. Note that the coupled peak power in the silicon nanowire is well below the TPA threshold at ~39 dBm.

After FWM, the idler DWDM signal in the L-band is isolated using a C/L-band splitter and then amplified using an L-band erbium doped fiber amplifier (EDFA). The individual DWDM channels are extracted using an optical tunable filter (OTF) (Santec, model OTF-350). The OTF transfer function has a 3-dB and 20-dB bandwidth of 0.14 nm and 0.29 nm, respectively. A plot of the transfer function can be found in Fig. 5(b). After extraction by the OTF, the BER performance of each DWDM channel is measured in a 10 Gbit/s pre-amplified receiver (Rx). In the case of DPSK, a 1-bit delay-interferometer (DLI) and balanced photo-detection (BPD) are employed. In the case of OOK, single-ended photo-detection is used. Note that the inclusion of two EDFAs between the FWM medium and the photo-detection are required due to a low FWM conversion efficiency in the silicon nanowire. With significantly higher conversion efficiency such as obtainable in the HNLF, a single EDFA placed either before or after the OTF should suffice. In this experiment, however, the configuration is kept identical in the HNLF case for ease of comparison between the results. We envisage an ideal system where the output DWDM signal of the FWM medium is amplified by a single EDFA, followed by WDM demultiplexing using an arrayed waveguide grating (AWG), and finally direct detection of each channel (assuming a sufficient FWM conversion efficiency).

It should be noted that the WSSs are used to fine-tune the amount of dispersion imposed onto both the OTDM and pump signals. The total dispersion depends not only on the used DCFs, but also on the various other components in the setup through which the signals propagate. The dispersion is optimised based on the DWDM spectrum obtained after FWM. Furthermore, the third-order dispersion of the 150 m DCF and 65 m DCF are compensated

#157928 - $15.00 USD Received 9 Nov 2011; revised 30 Nov 2011; accepted 1 Dec 2011; published 6 Dec 2011

using WSS1 and WSS2, respectively. Indeed, the third-order dispersion in the dispersive media can introduce distortions in the OFT, in particular for pump and data signals occupying relatively large bandwidths [14]. The observed effect of this compensation was negligible in our case, both on the DWDM spectrum and the BER performance, but a precise characterisation of the influence was not carried out.

4. Experimental results – silicon nanowire

The results of the OTDM-DWDM conversion in the silicon nanowire are shown in Fig. 5. The output spectrum of the silicon waveguide after FWM is shown in Fig. 5(a). The conversion efficiency of the FWM process is −32 dB. Note that the spectrum in (a) is obtained from the monitor output of a coupler and is not to scale (the optical spectrum analyzer noise floor is at −80 dBm). A spectrum of the central DWDM channels is shown in Fig. 5(b), both for a 640 Gbit/s and 160 Gbit/s OTDM rate at the same average input power. A successful OFT mapping of the 10 Gbit/s Gaussian pulse tributaries from 640 Gbit/s OTDM to individual 25 GHz spaced spectral channels can be observed. The Gaussian shape of the individual DWDM channels is apparent from the 100 GHz spaced DWDM channels obtained when reducing the OTDM bit rate to 160 Gbit/s. The transfer function of the OTF used to extract the individual DWDM channels is also shown (attenuation relative to peak, cf. right axis). It should be noted that the wavelength positions of the individual DWDM channels are shifted when changing the relative timing between pump and OTDM signal at the input to the FWM medium, while the envelope of the DWDM spectrum is unchanged. For the BER evaluation, the DWDM channels are held fixed by maintaining constant relative pump-OTDM timing, and each DWDM channel is extracted by tuning the OTF. Temperature fluctuations in the fibers before combination of the pump and OTDM signals cause slight variations in their relative timing, but these shifts are continuously compensated by small manual readjustments of the variable time-delay Δt, shown in Fig. 2(b). Similarly, temperature fluctuations in the fiber-based MUX stages resulted in small temporal variations of the OTDM tributary spacing, which converted into the small DWDM channel spacing variations observable in Fig. 5(b).

Figure 5(c) shows the BER curves of selected DWDM channels, and Fig. 5(d) shows the entire DWDM spectrum and the BER of each channel measured at a received power (P_{rec}) of −30 dBm. The 10 Gbit/s reference curve in (c) is measured on a 50% RZ-DPSK signal, obtained from a 1579 nm CW laser followed by the 10 Gbit/s MZM and a 10 GHz MZ pulse carver. As can be seen in Fig. 5(d), a total of 40 consecutive DWDM channels have a BER performance below the standard FEC threshold of 2×10^{-3}. The average channel spacing is 24.65 GHz. As expected, the best performance is obtained for the center channels originating from OTDM tributaries fully overlapped by the flat-top pump pulse, while the performance deteriorates for channels towards the sides of the DWDM spectrum originating from tributaries crossing the tails of the pump pulse. BER curves and received eye diagrams of channels corresponding to both cases can be found in Fig. 5(c) and (e), respectively. For example, the central 1579.41 nm case is among the best performing channels which achieve a BER just below 10^{-5}. On the other hand, the edge DWDM channel at 1583.65 nm does not achieve a BER below the FEC limit. The observed error-floor for all channels is attributed to an OSNR limitation. The limited FWM conversion efficiency of −32 dB of the silicon

#157928 - $15.00 USD Received 9 Nov 2011; revised 30 Nov 2011; accepted 1 Dec 2011; published 6 Dec 2011

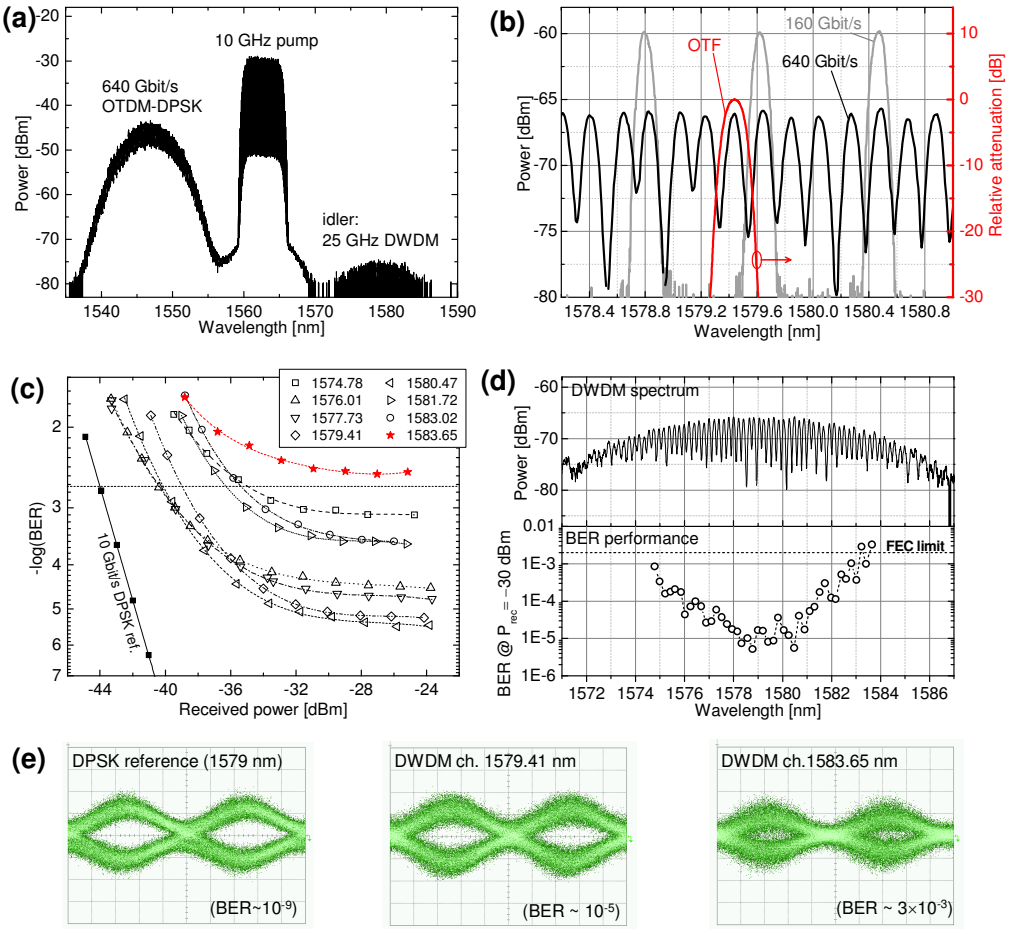

Fig. 5. Results for silicon nanowire. (a) Output spectrum of silicon nanowire, (b) zoom-in on idler DWDM spectrum in the cases of 160 Gbit/s and 640 Gbit/s OTDM input (left axis) and OTF transfer function (right axis), res. 0.01 nm, (c) 10 Gbit/s DPSK BER curves for selected DWDM channels, (d) DWDM spectrum (above) and BER performance of each DWDM channel at P_{rec} = –30 dBm (below), (e) received 10 Gbit/s demodulated DPSK eye diagrams.

nanowire results in a very low output DWDM power of the converter, leading to a low OSNR at the output of the subsequent EDFAs and a BER limitation at 10^{-5}. Assuming FEC can be applied, the demonstrated BER performance allows for a net error-free OTDM data rate of 595 Gbit/s after subtraction of a 7% FEC overhead. However, we expect that significantly better results can be obtained using silicon waveguides with lower propagation loss and therefore higher FWM conversion efficiency [7]. Indeed, the propagation loss of 4.3 dB/cm of our sample is relatively high compared to the state-of-the-art loss of ~1 dB/cm [18]. The use of such silicon nanowires are expected to yield significantly improved BER performance for this OTDM-DWDM conversion technique.

5. Experimental results – HNLF

The significantly higher FWM conversion obtainable in the HNLF leads to error-free performance with low power penalties for the OTDM-DWDM conversion. Figure 6 shows the results for the conversion of 640 Gbit/s OTDM-OOK to 25 GHz DWDM using the 50 m HNLF.

#157928 - $15.00 USD Received 9 Nov 2011; revised 30 Nov 2011; accepted 1 Dec 2011; published 6 Dec 2011

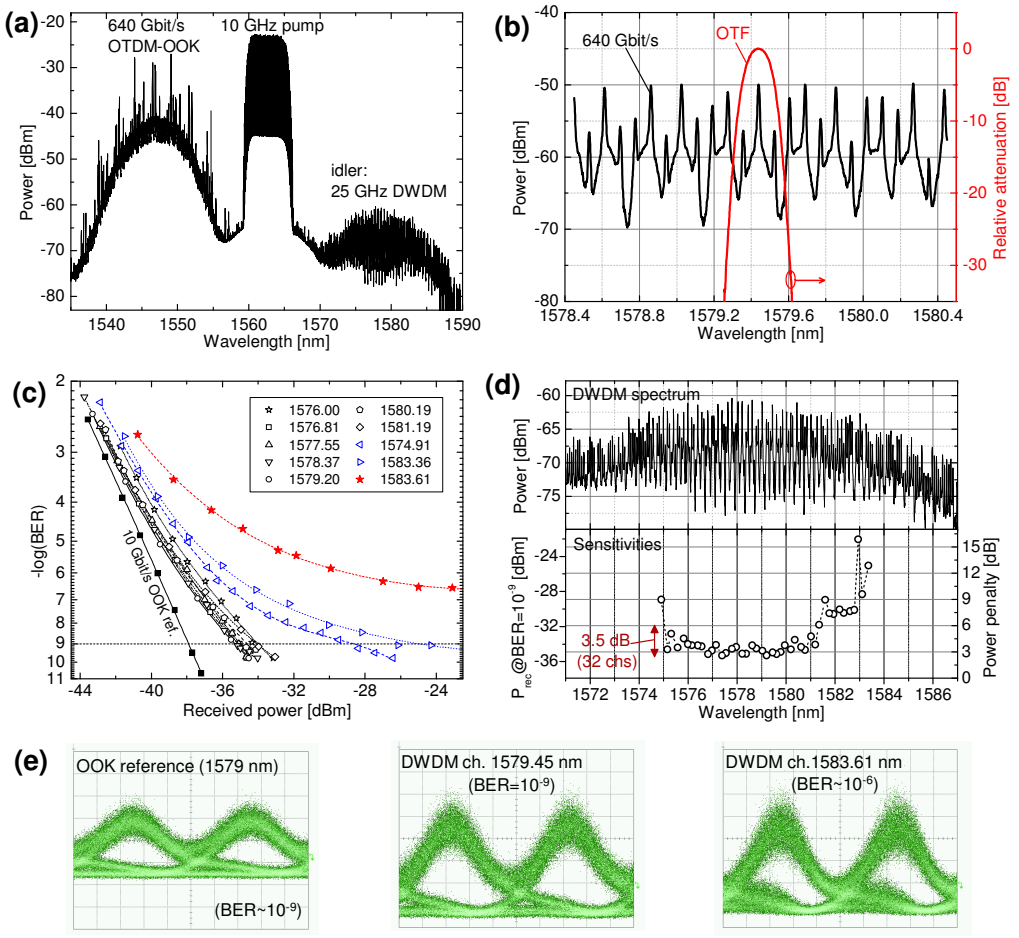

Fig. 6. Results for HNLF. (a) Output spectrum of HNLF, (b) zoom-in on idler DWDM spectrum with plot of OTF transfer function, res. 0.01 nm, (c) 10 Gbit/s OOK BER curves for selected DWDM channels, (d) DWDM spectrum (above) and sensitivity of each DWDM channel (required P_{rec} for BER = 10^{-9}) (below), (e) received 10 Gbit/s OOK eye diagrams.

The output spectrum of the HNLF after FWM is shown in Fig. 6(a). In this case, the FWM conversion efficiency is −24 dB, an improvement of 8 dB compared to the silicon nanowire using the same input powers. The resulting higher OSNR in the DWDM signal allowed for error-free performance using OOK instead of DPSK. Conversion of 640 Gbit/s OTDM-DPSK was not performed in the HNLF case. A close-up on the DWDM spectrum is shown in Fig. 6(b), together with the transfer function of the OTF. About nine 10 Gbit/s OOK DWDM channels with characteristic 10 GHz modulation peaks can be observed. In total, 43 consecutive channels extracted using the OTF have error-free performance (BER<10^{-9}). The average channel spacing is 24.41 GHz. The BER curves of selected DWDM channels are shown in Fig. 6(c). Figure 6(d) shows the entire DWDM spectrum and the sensitivities of the 43 error-free channels (the sensitivity is the required P_{rec} for a BER of 10^{-9}). The power penalty at BER = 10^{-9} relative to the 10 Gbit/s 50% RZ-OOK reference at 1579 nm is shown on the right axis. The majority of DWDM channels from ~1575 nm to ~1581 nm exhibit similar performance, which is attributed to the flat-top pump pulse allowing for a linear chirp and uniform conversion efficiency over a broad time-span of ~83 ps. In particular, the 32 channels (half of all tributaries) ranging from 1575.2 nm to 1581.4 nm have power penalties within a 3.5 dB interval, ranging from 2.5 dB to 6 dB compared to the 10 Gbit/s reference.

#157928 - $15.00 USD Received 9 Nov 2011; revised 30 Nov 2011; accepted 1 Dec 2011; published 6 Dec 2011

Figure 6(c) shows BER curves (in black) of various DWDM channels within this group, and a corresponding OOK eye diagram is shown in Fig. 6(e), middle. The BER curves of the first (1574.91 nm) and last (1583.36 nm) DWDM channel for which error-free performance is obtained are shown in blue. A large penalty is obtained, which is attributed primarily to the expected DWDM inter-channel cross-talk in this part of the DWDM spectrum, rather than to an OSNR limitation. Indeed, the eye diagram of the following 1583.61 nm channel in Fig. 6(e), right, shows a closure with clear indication of inter-channel cross talk. The corresponding BER curve in Fig. 6(c) (in red) has an error floor above 10^{-7}.

An asymmetry can be observed in the sensitivity vs. DWDM channel plot in Fig. 6(d), where a small group of channels in the range 1581.5 nm to 1583 nm display shifted sensitivities. We expect the asymmetric behavior to result from a deviation of the employed pump pulse from the ideal case of a symmetric intensity profile and a constant linear chirp rate *K/2*. This is indicated by the measured OSO trace in Fig. 3(b), where a slight asymmetry with a small ripple appearing on the right shoulder can be observed (the chirp profile of the pulse could not be measured). The OTDM tributaries exposed to a pump intensity ripple and/or a deviation of the chirp rate from the OFT condition will become distorted in the conversion process, resulting in a deteriorated BER performance. We expect that an ideally chirped super-Gaussian pump pulse will result in a DWDM signal with a more uniform channel performance compared to the results obtained in the present demonstration. Indeed, preliminary numerical simulations of our set-up (HNLF case) employing the ideal 5th order super-Gaussian pump profile indicate that 42 OTDM tributaries can be converted to 25 GHz spaced DWDM channels with both a power variation and sensitivity variation within 1 dB. We plan to publish the detailed results of these simulations in a future paper.

6. Conclusion

For the first time, we have demonstrated optical serial-to-parallel conversion with high spectral efficiency by converting ultra high-speed OTDM data to dense WDM data, using both a 3.6 mm silicon nanowire and a 50 m HNLF. The conversion is based on time-domain OFT by FWM, allowing for the conversion of more than half of all OTDM tributaries in a single device. Using the silicon nanowire for FWM, 40 out of 64 tributaries of a 64 × 10 Gbit/s OTDM-DPSK signal were converted to 25 GHz DWDM with a BER performance within FEC limits. Improved BER performance is expected for silicon waveguides with lower propagation loss and consequently higher FWM conversion efficiency. Using the HNLF to obtain a higher FWM conversion efficiency, 43 out of 64 tributaries of a 64 × 10 Gbit/s OTDM-OOK signal were converted to 25 GHz DWDM with error-free BER performance.

The demonstrated technique enables a full and spectrally efficient demultiplexing of an ultra-high-speed serial OTDM signal using only two nonlinear OFT devices. Compared with standard single-tributary demultiplexers, the OFT technique allows for a strongly simplified OTDM receiver with potentially much lower energy consumption.

Acknowledgments

We would like to acknowledge OFS Fitel Denmark ApS for kindly providing the highly nonlinear fibers used in the experiments. The Danish Research Council is acknowledged for supporting the NOSFERATU project and the European Research Council for supporting the SOCRATES project.

#157928 - $15.00 USD Received 9 Nov 2011; revised 30 Nov 2011; accepted 1 Dec 2011; published 6 Dec 2011